Combustion and Flame 205 (2019) 80–92

Contents lists available at ScienceDirect

Combustion and Flame

journal homepage: www.elsevier.com/locate/combustflame

High-pressure pyrolysis and oxidation of DME and DME/CH_4

Hamid Hashemi*, Jakob M. Christensen, Peter Glarborg

DTU Chemical Engineering, Technical University of Denmark, Lyngby DK-2800, Denmark

ARTICLE INFO

Article history:
Received 31 August 2018
Revised 26 October 2018
Accepted 20 March 2019
Available online 5 April 2019

Keywords:
Dimethyl ether (DME)
Methane
Oxidation
High pressure
Reaction mechanism
F
Intermediate temperatures
F

ABSTRACT

The pyrolysis and oxidation of dimethyl ether (DME) and its mixture with methane were investigated at high pressure (50 and 100 bar) and intermediate temperature (450–900 K). Mixtures highly diluted in nitrogen with different fuel–air equivalence ratios ($\Phi = \infty$, 20, 1, 0.06) were studied in a laminar flow reactor. At 50 bar, the DME pyrolysis started at 825 K and the major products were CH_4, CH_2O, and CO. For the DME oxidation at 50 bar, the onset temperature of reaction was 525 K, independent of fuel–air equivalence ratio. The DME oxidation was characterized by a negative temperature coefficient (NTC) zone which was found sensitive to changes in the mixture stoichiometry but always occurring at temperatures of 575–625 K. The oxidation of methane doped by DME was studied in the flow reactor at 100 bar. The fuel–air equivalence ratio (Φ) was varied from 0.06 to 20, and the DME to CH_4 ratio changed over 1.8–3.6%. Addition of DME had a considerable promoting effect on methane ignition as the onset of reaction shifted to lower temperatures by 25–150 K. A detailed chemical kinetic model was developed by adding a DME reaction subset to a model developed in previous high-pressure work. The model was evaluated against the present data as well as data from literature. Additional work is required to reconcile experimental and theoretical work on reactions on the CH_3OCH_2OO PES with ignition delay measurements in the NTC region for DME.

1. Introduction

The steady increase in the global energy demand along with the release of carbon dioxide and harmful pollutants from the combustion of fossil fuels are the major motivations to seek alternative sources of energy. In medium term, fuels which produce less pollutants and have a higher energy efficiency may relieve the environmental problems to some extent. Among the alternative fuels, dimethyl ether (DME) has attracted interest, especially for use in engines. DME can be produced from different feedstocks, e.g., oil, natural gas, coal, biomass, and waste products. Bio-derived DME fuel can potentially reduce the CO_2 load on the environment. Lower ignition temperature, shorter ignition delay time, and easier evaporation compared to conventional diesel fuels make DME an attractive alternative. Replacing diesel fuel by DME reduces the emission of particulate matter (PM) and nitrogen oxides (NO_x) from slightly modified compression-ignition (CI) engines [1–5]. The absence of a C–C bond in the molecular structure of DME, as well as its content of oxygen, is believed to suppress soot formation [2]. DME can also replace natural gas in slightly modified gas turbines [6]. However, the relatively low energy density and the potentially increased emission of aldehydes and CO may challenge widespread usage of DME as a fuel [2].

DME has also been considered as an additive to improve combustion properties of fuels such as natural gas. Adding DME to natural gas or methane accelerates ignition [7–11], increases the flame speed [8,12], and alter extinction limits [13]. Furthermore, DME addition can suppress the formation of polycyclic aromatic hydrocarbons (PAHs) and soot [14] and reduce NO_x emissions [15]. DME is also an effective additive in ethanol-fueled CI and SI (spark-ignition) engines [16,17]. DME was considered as an additive to methanol for use in CI engines in early studies [18–20]. Whereas DME accelerates methane ignition, its effect on ethane oxidation is more complicated [21]. Therefore there is an incentive to understand interactions between DME and the components of natural gas, especially since local variations in the composition of natural gas can be noticeable.

The DME ignition and oxidation show a complicated behavior with a negative temperature coefficient (NTC) at intermediate temperatures [22–25]. Ignition in engines is greatly affected by combustion chemistry at high pressure and intermediate temperature. Moreover, the low-temperature fuel chemistry affects significantly the turbulent flame and its propagation velocity [26]. Studies in the high-pressure, medium temperature regime are usually limited to flow reactors and rapid compression machines (RCM), but for DME shock tubes are also useful due to its short

* Corresponding author.
E-mail address: hah@kt.dtu.dk (H. Hashemi).

https://doi.org/10.1016/j.combustflame.2019.03.028
0010-2180/

ignition delay time. Most reported shock-tube studies have been limited to pressures below 30 bar [9,10,27,28], but Pfahl et al. [22] measured ignition delays at pressures up to 40 bar, reasserting the two-stage ignition of DME. DME flame-measurements were conducted at pressures as high as 10–20 bar [29–31], but they mostly reflect the high-temperature oxidation chemistry of DME.

Ignition delays and flame speeds are valuable as benchmarks in kinetic studies, but for details of the oxidation chemistry species profiles upon ignition from flow reactors offer useful information. Dagaut et al. [23,32] used a jet-stirred reactor (JSR) to study DME oxidation at pressures up to 10 atm. More recently, Rodriguez et al. [33] studied DME oxidation in an atmospheric jet-stirred reactor at 550–1100 K. Moshammer et al. [34] coupled a jet-stirred reactor with molecular-beam sampling capabilities to detect $HOOCH_2OCHO$, methyl formate, formic acid and some other components in DME oxidation at a low temperature of 540 K. DME oxidation in flow reactors were investigated at atmospheric pressure by Herrmann et al. [35,36] and Kurimoto et al. [37], and by Dryer and coauthors [24,25,38,39] at pressures below 20 atm. Very recently, Marrodán et al. [40] investigated DME oxidation at 450–1050 K and 20–60 bar, focusing on its interaction with NO_x.

Despite its importance, results on interactions of DME with natural gas components are still rare. Flow-reactor measurements of CH_4/DME oxidation have been reported by Sen et al. [11] (6 atm and 532–992 K) and Amano and Dryer [7] (10–18 atm and 800–1060 K). Burke et al. [28] measured ignition delays of CH_4/DME mixtures over 10–30 atm and 600–1400 K, while Dames et al. [41] reported data for C_3H_8/DME mixtures at 10–50 atm and 550–2000 K Other studies of DME addition to natural gas components, e.g., [8–10,12], were mostly limited to temperatures above 1000 K. Extending data to high pressure and intermediate temperature is beneficial in understanding CH_4/DME interactions.

Developing chemical kinetic models for combustion of methane and DME is a vital step in utilizing their mixtures practically. Early models for DME oxidation were proposed by Dagaut et al. [23,32] and by Alzueta et al. [42], based on data from jet-stirred reactors (JSR) and atmospheric flow reactors, respectively. In a series of papers, Curran and coworkers [24,25,38,43] established a DME mechanism, based on modeling of data from flow reactors and RCM. This model was recently updated to improve the predictive capabilities at high pressure [28]. Studies of ignition and oxidation of mixtures of CH_4 and DME [7–10,12,13] have to a significant extent relied on the models for neat DME oxidation.

In this work, we present the results of DME pyrolysis and oxidation at 50 bar as well as results of tests on methane doped with DME at 100 bar, all at 450–900 K. All experiments are conducted in a laminar flow reactor under conditions ranging from strongly reducing to very oxidizing. A DME reaction subset is established by individual evaluation of thermodynamic properties and elementary reactions. This subset is added to a base model developed earlier for hydrogen, hydrocarbons, and alcohols and carefully validated for high-pressure conditions [44–49]. Modeling predictions are compared with the present data and results from the literature. The first-principles approach to modeling adopted in this work is different from that taken in literature, where mechanisms are generally tuned to improve accuracy. The DME oxidation chemistry is so complex that tuning rate constants to achieve a better fit to available experimental data sets is unlikely to lead to unique parameterizations [50]. Furthermore, rate constants commonly used in modeling for some of the key reactions, that of CH_3OCH_2 with O_2 and the subsequent steps of $CH_2OCH_2O_2$ and $CH_2OCH_2O_2H$, appear to conflict with recent experiments and master equation calculations [51,52].

2. Experimental approach

The experimental setup was a laboratory-scale high-pressure laminar-flow reactor designed to approximate plug flow [53]. The setup has been described in detail elsewhere [53] and only a brief description is provided here. The system was used here to study the oxidation chemistry of DME as well as its mixture with methane. The temperature of the reactor was varied between 450 and 900 K. The DME experiments were conducted at 50 bar pressure and with a constant flow rate of 4.53 NL/min (STP; 1 atm and 273 K). The residence time of gases in the hot isothermal zone of the reactor was between 4.1 and 9.1 s. The oxidation of methane doped by DME was studied at 100 bar and at a flow rate of 3.23 NL/min (STP), resulting in gas residence times between 10.6 and 21.8 s.

The reactions took place in a tubular quartz reactor (inner diameter of 8 mm) to minimize the effects of surface reactions. The quartz reactor was enclosed in a stainless steel tube that acted as a pressure shell. The system was pressurized from the feed gas cylinders and the reactor pressure was controlled by a pneumatically operated pressure control valve positioned after the reactor. The pressure fluctuations of the reactor were limited to $\pm 0.2\%$.

The steel tube was placed in a tube oven with three individually-controlled electrical heating-elements that produced an isothermal reaction zone (± 6 K) of $\sim$37–41 cm in the middle of the reactor. A moving thermocouple was used to measure the temperature profile inside the pressure shell at the external surface of the quartz tube after stabilizing the system.

The flow rates of different gases were regulated by mass-flow controllers. The gases were mixed at ambient temperature well before entering the reactor. All gases used in the present experiments were high purity gases or mixtures with certified concentrations ($\pm 2\%$ uncertainty). The total flow rate was measured by a bubble flow meter downstream of the reactor. Using a quartz tube and conducting experiments at high pressures were expected to minimize the contribution from heterogeneous reactions at the reactor wall.

Downstream of the reactor, the system pressure was reduced to atmospheric level prior to product analysis, which was conducted by an on-line *6890N Agilent Gas Chromatograph* (GC-TCD/FID) calibrated according to the procedure in [45]. GC measurements were conducted at least twice for each temperature and the average is shown. The GC allowed detection of O_2, CO, CO_2, CH_4, C_2H_4, and C_2H_6 with estimated uncertainties around 5%. Distinguishing methanol from acetaldehyde was not possible due to signal overlap in the GC detector. However, it was possible to measure the signal areas corresponding to the sum of these components. According to simulations, no yield of acetaldehyde was expected in the present experiments, so the sum of acetaldehyde and methanol could be interpreted and quantified as methanol. Moreover, an increased uncertainty of about 20% is assigned to the measurement of formaldehyde due to the small signal to noise ratio of formaldehyde.

For each set of experiment, the mole fractions of reactants as well as the gas pressure were constrained while the temperature of the isothermal zone was increased in small steps which simultaneously shortened the gas residence time in the reactor.

Figure 1 shows the measured temperature profiles for a nitrogen flow with flow rate and pressure corresponding to the DME experiments. The tabulated temperature profiles for the DME experiments can be found in supplementary data. For the doped methane experiments, the temperature profiles were similar to those reported by Hashemi et al. [45]. During this work, it was found that considering only the isothermal zone of the reactor in interpreting and simulating the data could be misleading, due to the considerable reactivity of DME at the low temperatures in the

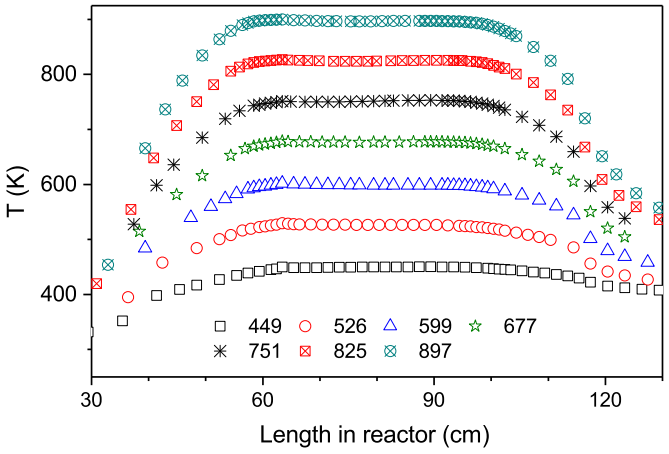

Fig. 1. Measured temperature profiles across the reaction zone. The flow was pure nitrogen with a flow rate of 4.53 NL/min at a pressure of 50 bar.

heating zone of the reactor. Therefore, a plug flow approximation with constrained temperature according to the measured profiles was used for modeling in Chemkin [54].

Selected experiments under oxidizing conditions were repeated after a few weeks, and the results agreed within the stated error range. The reactants were strongly diluted in inert gas to limit the temperature rise due to exothermic reactions. Simulations with a constant pressure and enthalpy (adiabatic) model lead to a maximum temperature rise of 5 K for neat DME experiments and 25 K for the mixtures of methane and DME. The narrow quartz tube used here accelerated the thermal equilibrium between the reactive gas inside the reactor and the heating bath gas surrounding it, so the deviation of the gas temperature from the measured profiles is estimated to be even smaller.

3. Chemical kinetic model

The chemical kinetic model was based on $H_2/C_1/C_2$/alcohols submodels developed recently for high-pressure conditions [44–49]. The oxidation subset for formic acid was taken from the study by Marshall and Glarborg [55]. The DME reactions were evaluated one-by-one and the most reliable rate constants were adopted. Tuning of rate constants was avoided, so the model can reflect better the status of our knowledge of DME combustion chemistry at intermediate temperature and high pressure. The most important reactions are listed in Table 2 and are reviewed below. Details of other reactions can be found in the supplementary material.

3.1. Thermodynamic properties

Thermodynamic properties for most species were drawn from the database of Burcat and coworkers [56], as discussed in earlier work [44–49]. Table 1 lists the thermodynamic properties for selected species considered in the current model. Most of these species were added to the mechanism in the present work, as part of the DME subset. Only few of them were covered by the Burcat database, and data were drawn also from calculation [57] and estimation [28,58]. For some intermediate species, notably CH_3OCH_2OO, CH_2OCH_2OOH, CH_3OCH_2O, OCH_2OCHO, and CH_3OCO, the enthalpy of formation differs considerably among the reviewed sources (see Supplementary material for further details). While these differences have only a minor effect on the model predictions for the high-pressure flow reactor conditions, they might be important under other conditions and more work on the thermodynamic properties of the DME subset is desirable.

3.2. DME subset

An accurate description of the thermal decomposition of DME is needed in modeling its pyrolysis and high temperature oxidation.

$$CH_3OCH_3 = CH_3 + CH_3O \quad (R1)$$

Sivaramakrishnan et al. [59] combined shock-tube measurements with theoretical calculations to derive pressure-dependent rate constants of DME dissociation over 500–2000 K and at pressures of 0.01–300 bar. We have adopted their calculated rate constant for R1; a roaming channel to $CH_4 + CH_2O$ was predicted to be negligible. More recently, Tranter et al. [60] measured the title reaction over temperatures of 1500–2450 K and at low pressures, supporting the theoretical rate constant at least for temperatures below 1800 K.

Reactions of DME with radicals are generally well characterized. The reaction between DME and atomic hydrogen (R2) was investigated experimentally by Sivaramakrishnan et al. [59] at 1149–1465 K.

$$CH_3OCH_3 + H = CH_3OCH_2 + H_2 \quad (R2)$$

Combining their results with available data from literature, Sivaramakrishnan et al. [59] suggested a rate constant valid for temperatures of 273–1465 K. Hydrogen abstraction by hydroxyl,

$$CH_3OCH_3 + OH = CH_3OCH_2 + H_2O \quad (R4)$$

was explored by Carr et al. [61] at 200–850 K using laser flash-photolysis. They further extrapolated rate constants over 200–1400 K by utilizing theoretical calculations and adding data at lower and higher temperatures from literature. For the DME + methyl reaction,

$$CH_3OCH_3 + CH_3 = CH_3OCH_2 + CH_4 \quad (R7)$$

we rely on measurements by Tranter et al. [62] in a shock tube at low pressure and over 1163–1629 K.

Hydrogen abstraction from the fuel by peroxides has been shown to be important for low temperature, high pressure oxidation of both C_1–C_3 alkanes [45,46,63] and alcohols [47,49]. Unfortunately, the DME + peroxide reactions are not well characterized. For the DME + HO_2 reaction,

$$CH_3OCH_3 + HO_2 = CH_3OCH_2 + H_2O_2 \quad (R5)$$

we adopt the rate suggested by Mendes et al. [64] from a theoretical study. It should be noted that this value is considerably smaller than that proposed by Zhao et al. [24]. The H-abstraction from the fuel by CH_3OO (R10) was assumed to be a factor of five lower than $CH_3OCH_3 + HO_2$ (R5), consistent with the ratio between $CH_4 + CH_3OO$ and $CH_4 + HO_2$ [65].

The hydrogen abstraction by O_2 (R6) is a potential initiating step in intermediate temperature oxidation of DME.

$$CH_3OCH_3 + O_2 = CH_3OCH_2 + HO_2 \quad (R6)$$

The reaction likely proceeds in the backward direction at later stages of oxidation and acts as a sink for radicals. The rate for R6 is estimated by analogy to $CH_3OH + O_2$.

The fate of the methoxymethyl radical is important in predicting oxidation behavior and ignition delay times for DME. In the current temperature range, dissociation of CH_3OCH_2 competes with its reaction with O_2. For the dissociation (R13), we adopt the rate coefficients derived from RRKM calculations by Burke et al. [28].

$$CH_3OCH_2 = CH_2O + CH_3 \quad (R13)$$

The determination from Burke et al. is in better agreement with the early experimental results [66,67] than the more recent theoretical rate constant from Gao et al. [68].

Table 1
Adopted thermodynamic properties of selected species in DME subset. Units are *kcal/mol* for H, *K* for temperature, and *cal/(mol K)* for S and C_p.

Species	H_{298}	S_{298}	$C_{p,300}$	$C_{p,400}$	$C_{p,600}$	$C_{p,800}$	$C_{p,1000}$	$C_{p,1500}$	Ref.
CH_3OCH_3	−43.96	63.89	15.79	18.97	25.16	30.03	33.80	39.46	[56]
CH_3OCH_2	0.73	67.38	15.50	18.42	23.39	27.54	30.59	34.95	[57]
CH_3OCH_2OO	−36.19	82.91	22.06	25.93	32.19	36.82	40.21	45.33	[28]
CH_2OCH_2OOH	−25.52	85.67	21.72	26.36	33.06	37.39	40.32	45.15	[28]
CH_3OCH_2OOH	−69.36	83.39	22.68	27.52	34.98	40.21	43.95	49.73	[28]
CH_3OCH_2O	−39.96	73.89	18.27	21.05	26.54	31.43	35.33	40.61	[28]
OCH_2OCHO	−81.71	76.71	17.74	21.40	27.36	31.69	34.66	38.13	[28]
$HOOCH_2OCHO$	−111.11	86.21	22.88	27.75	35.23	40.33	43.71	47.94	[28]
CH_3OCHO	−85.51	68.40	14.97	17.94	23.75	28.02	31.22	35.90	[56]
CH_3OCH_2OH	−89.43	71.65	20.44	25.99	33.43	37.03	39.79	45.01	[58]
$OOCH_2OCH_2OOH$	−61.71	101.04	29.34	34.76	42.67	47.75	51.08	56.05	[28]
$HOCH_2OCO$	−83.86	79.01	18.57	21.20	26.34	30.80	34.20	38.30	[28]
CH_2OCHO	−37.42	70.61	14.64	17.57	22.62	26.52	29.28	32.46	[28]
CH_3OCO	−37.87	70.57	15.23	17.87	22.29	25.95	28.48	31.62	[57]

The $CH_3OCH_2 + O_2$ reaction has been investigated experimentally and theoretically by Eskola et al. [51], who conducted their study at temperatures of 195–650 K and at sub-atmospheric pressures (0.007–0.7 bar). They identified three product channels for the reaction,

$$CH_3OCH_2 + O_2 = CH_3OCH_2OO \quad (R14a)$$

$$CH_3OCH_2 + O_2 = CH_2OCH_2OOH \quad (R14b)$$

$$CH_3OCH_2 + O_2 = CH_2O + CH_2O + OH \quad (R14c)$$

The measured rate constants were extrapolated to 200–1000 K and elevated pressure using master equation simulations. The Eskola value of k_{14a} is in excellent agreement with the determination of Sehested et al. [67], obtained at 18 bar. We fitted logarithmic pressure-dependent rate constants based on the Chebyshev polynomial rate expressions reported by Eskola et al. [51].

Reaction R14a is followed by isomerization or dissociation of CH_3OCH_2OO (R15),

$$CH_3OCH_2OO = CH_2OCH_2OOH \quad (R15a)$$

$$CH_3OCH_2OO = CH_2O + CH_2O + OH \quad (R15b)$$

The competition between these two channels has a strong impact on chain-branching at lower temperatures. Based on their measurements and master equation calculations, Eskola et al. [51] derived temperature and pressure dependencies for k_{15a} and k_{15b}.

A global uncertainty propagation and sensitivity analysis for the $CH_3OCH_2 + O_2$ system indicate that the rate coefficients for R14 and R15 from Eskola et al. are accurate within a factor of three or better [52]. However, the Eskola values deviate significantly from values used in modeling [13,24,28,33,40,41]. Figure 2 compares rate constants for reactions on the CH_3OCH_2OO potential energy surface. While the values from Burke et al. [28] have been shown to provide a superior overall performance against a wide range of experimental targets [41], they appear to be incompatible with the results of Eskola et al. [51] and Shannon et al. [52].

The internal H-abstraction in R15a yields CH_2OCH_2OOH, which adds to molecular oxygen to give $OOCH_2OCH_2OOH$,

$$CH_2OCH_2OOH + O_2 = OOCH_2OCH_2OOH \quad (R19)$$

The rate constant for R19, as well as that for the decomposition of $OOCH_2OCH_2OOH$ (R21), was calculated by Burke et al. [28]. $HOOCH_2OCHO$, formed in R21, dissociates via OH elimination [25], $HOOCH_2OCHO = OCH_2OCHO + OH$ (R22). A secondary dissociation channel forming the Criegee intermediate CH_2OO and formic acid [69,70] is probably of minor importance. OCH_2OCHO formed in R22 dissociates to form primarily $HOCHO + HCO$ (R23) [41].

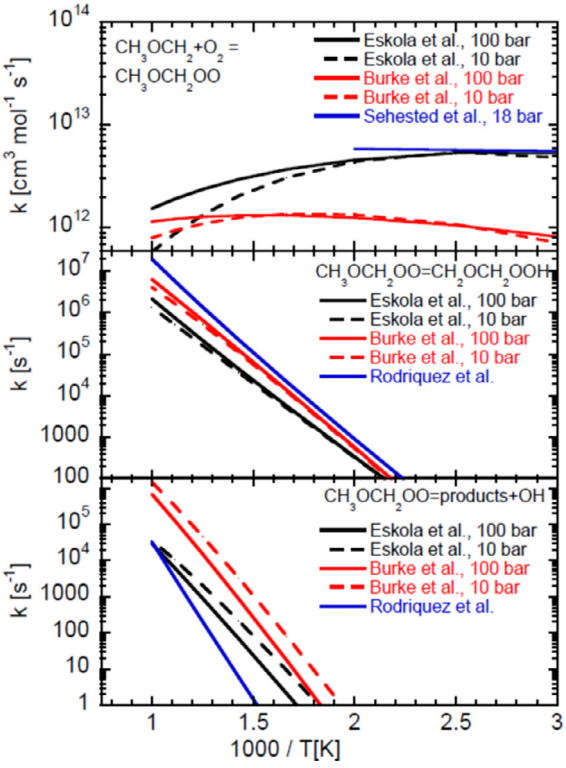

Fig. 2. Arrhenius plot for reactions on the CH_3OCH_2OO potential energy surface. Rate constants are drawn from Eskola et al. [51], Burke et al. [28], Sehested et al. [67], and Rodriquez et al. [33].

Formic acid (HOCHO) and methyl formate (CH_3OCHO) are important intermediates in DME oxidation. For formic acid, we adopted the reaction data from Marshall and Glarborg [55]. The methyl formate subset is mainly taken from Dooley et al. [71], but the reactions were updated whenever more reliable data were found.

4. Results and discussion

Species profiles from DME pyrolysis and oxidation in the flow reactor at intermediate temperatures (450–900 K) and high pressure (50 bar) will be presented in this section. Afterwards, the results of the oxidation experiments of methane doped by DME over 450–900 K and at 100 bar will be presented and compared with data for the neat methane oxidation published earlier [45]. To

Table 2
Selected reactions from the DME chemical kinetic model. The rate constants are in the form of $k = AT^n \exp(-E/(RT))$. Units are mol, cm, K, s, and cal.

	Reaction	A	n	E	Note/Ref.
		Arrhenius data			
R1	$CH_3OCH_3 = CH_3 + CH_3O$	2.3E19	−0.66	84,092	[59][a]
R2	$CH_3OCH_3 + H = CH_3OCH_2 + H_2$	3.9E00	4.13	1779	[59]
R3	$CH_3OCH_3 + O = CH_3OCH_2 + OH$	4.2E13	0.00	5305	est[b]
R4	$CH_3OCH_3 + OH = CH_3OCH_2 + H_2O$	2.0E07	1.89	−365	[61]
R5	$CH_3OCH_3 + HO_2 = CH_3OCH_2 + H_2O_2$	3.2E−03	4.64	10,556	[64]
R6	$CH_3OCH_3 + O2 = CH_3OCH_2 + HO_2$	7.2E05	2.27	42,760	est[c]
R7	$CH_3OCH_3 + CH_3 = CH_3OCH_2 + CH_4$	1.0E01	3.78	9687	[62]
R8	$CH_3OCH_3 + HCO = CH_3OCH_2 + CH_2O$	9.8E−14	7.37	9731	est[d]
R9	$CH_3OCH_3 + CH_3O = CH_3OCH_2 + CH_3OH$	3.8E09	0.83	6334	[72]
R10	$CH_3OCH_3 + CH_3OO = CH_3OCH_2 + CH_3OOH$	6.3E−4	4.64	10,556	est[e]
R11	$CH_3OCH_3 + CH_3CH_2OO = CH_3OCH_2 + CH_3CH_2OOH$	5.1E−4	4.64	10,556	est[f]
R12	$CH_3OCH_3 + CH_3OCH_2OO = CH_3OCH_2 + CH_3OCH_2OOH$	7.0E−4	4.85	10,346	est[g]
R13	$CH_3OCH_2 = CH_2O + CH_3$	2.7E29	−4.94	31,786	[28][h]
R14a	$CH_3OCH_2 + O_2 = CH_3OCH_2OO$	1.4E22	−3.16	2183	[51][h,i]
R14b	$CH_3OCH_2 + O_2 = CH_2OCH_2OOH$	1.2E18	−2.33	4177	[51][h,i]
R14c	$CH_3OCH_2 + O_2 = CH_2O + CH_2O + OH$	1.2E10	0.15	6531	[51][h,i]
R15a	$CH_3OCH_2OO = CH_2OCH_2OOH$	2.7E02	2.33	14,168	[51][h,i]
R15b	$CH_3OCH_2OO = CH_2O + CH_2O + OH$	1.8E22	−3.47	33,781	[51][h,i]
R16a	$2CH_3OCH_2OO = CH_3OCH_2O + CH_3OCH_2O + O_2$	1.6E23	−4.50	0	[41]
R16b	$2CH_3OCH_2OO = CH_3OCHO + CH_3OCH_2OH + O_2$	6.8E22	−4.50	0	[41]
R17	$CH_3OCH_2O + OH = CH_3OCH_2OOH$	6.0E12	0.00	0	est [58]
R18	$CH_3OCH_2OO + HO_2 = CH_3OCH_2OOH + O_2$	1.8E10	0.00	−3273	est [58]
R19	$CH_2OCH_2OOH + O_2 = OOCH_2OCH_2OOH$	4.9E12	−0.32	428	[28]
R20	$CH_2OCH_2OOH = CH_2O + CH_2O + OH$	8.9E29	−6.05	20,964	[51][h,i]
R21	$OOCH_2OCH_2OOH = HOOCH_2OCHO + OH$	3.9E07	0.98	17,467	[28]
R22	$HOOCH_2OCHO = OCH_2OCHO + OH$	1.8E20	−1.58	38,876	est [58]
R23	$OCH_2OCHO = HOCHO + HCO$	4.2E14	−0.80	14,630	[41][h]
R24	$CH_2O + OCHO = OCH_2OCHO$	3.9E11	0.00	2500	[71]

[a] High-pressure limit, see the supplementary mechanism files for low-pressure limits and Troe parameters.
[b] Estimated as two times of the rate of $CH_3OH + O = CH_2OH + OH$.
[c] Estimated as two times of the rate of $CH_3OH + O_2 = CH_2OH + HO_2$.
[d] Estimated as two times of the rate of $CH_3OH + HCO = CH_2OH + CH_2O$.
[e] Estimated as 20% of $CH_3OCH_3 + HO_2$ (R5).
[f] Estimated as 16% of $CH_3OCH_3 + HO_2$ (R5).
[g] Estimated as two times of the rate of $CH_3OO + CH_3OH = CH_3OOH + CH_2OH$.
[h] At 100 atm pressure, see the supplementary mechanism files for other pressures.
[i] Fitted from the Chebyshev polynomial rate expressions.

simulate the flow-reactor in Chemkin [54], a plug flow approximation with constrained temperature (according to the provided temperature profiles in Supplementary material) and pressure is used. Also in Supplementary material, the flow reactor data are compared with predictions obtained using the mechanisms of Burke et al. [28] and Reuter et al. [13]; the level of agreement is similar to that obtained by the present model.

4.1. Pyrolysis and oxidation of neat DME in the flow reactor

Figure 3 shows results from the DME pyrolysis experiments. The DME dissociation starts around 825 K, where a trace amount of methane is detected. At higher temperatures, CH_2O and CO are detected as well. Carbon is balanced within ±3%. Although the model overpredicts slightly the conversion at high temperatures, the agreement is satisfactory. Under the conditions of these experiments, dissociation of DME (R1) is at the high pressure limit. The good agreement between experiment and modeling supports the estimate of $k_{1,\infty}$ proposed by Sivaramakrishnan et al. [59].

Under reducing conditions (Φ=20, Fig. 4), the DME consumption starts around 525 K, and CO is detected above 550 K. Between 575 K and 675 K, the concentration of DME remains almost constant, indicating NTC behavior. The presence of an NTC region is more pronounced in the oxygen profile at 575–625 K, where the oxygen level increases with temperature. Rapid DME oxidation resumes at higher temperatures and oxygen is completely consumed above 750 K. The major detected products are formaldehyde at low temperature and CO and CH_4 at higher temperatures.

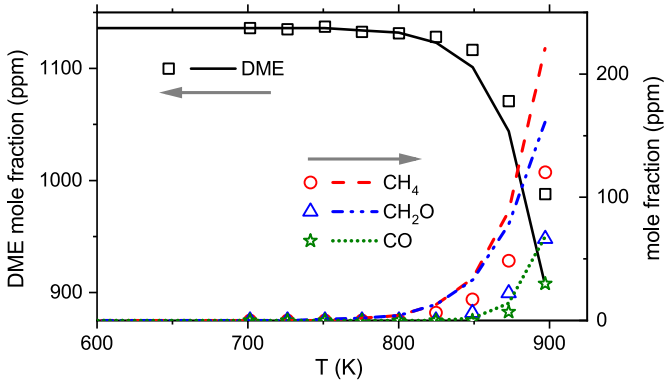

Fig. 3. Comparison of experimental and predicted concentration profiles as a function of the reactor temperature for pyrolysis of DME. The pressure was 50 bar, and the residence time in the isothermal zone was 4.1–9.1 s. The inlet composition was 1136 ppm DME in N_2. The symbols mark experimental data while solid lines denote model predictions obtained with the full temperature profile.

Trace amounts of ethene and ethane are also measured above 700 K.

The model predicts fairly well the complicated non-monotonic changes in species concentrations against temperature. The levels of CH_4 and CO are well reproduced, while C_2H_6 is underpredicted by a factor of two. The formaldehyde profile is captured qualitatively, but is only accurate within a factor of two.

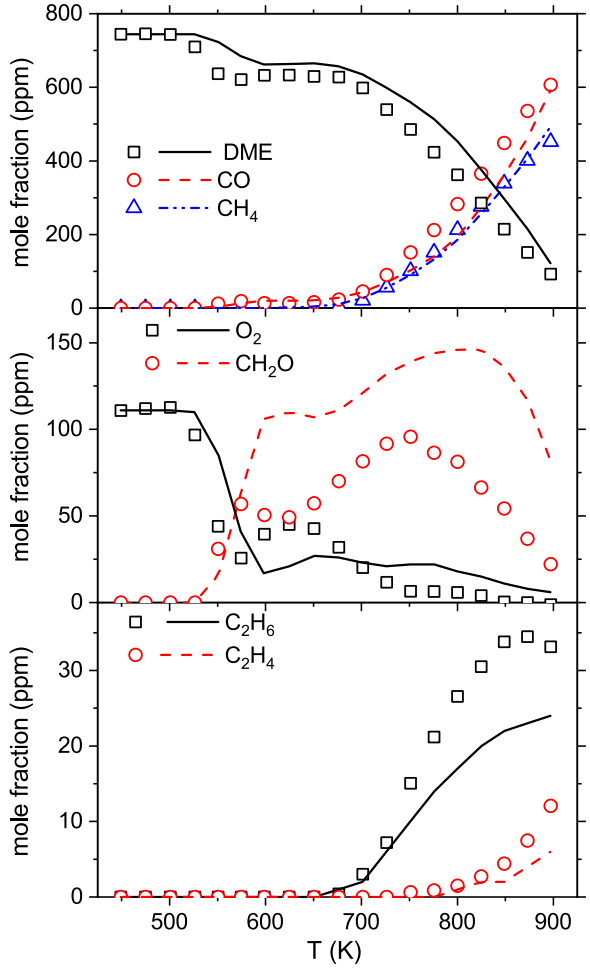

Fig. 4. Comparison of experimental and predicted concentration profiles as a function of the reactor temperature for the reducing experiment with DME/O_2 (Φ=20.2). The pressure was 50 bar, and the residence time in the isothermal zone was 4.1–9.1 s. The inlet composition was 744 ppm DME, 111 ppm O_2, and N_2 by difference. The symbols mark experimental data while solid lines denote model predictions obtained with the full temperature profile.

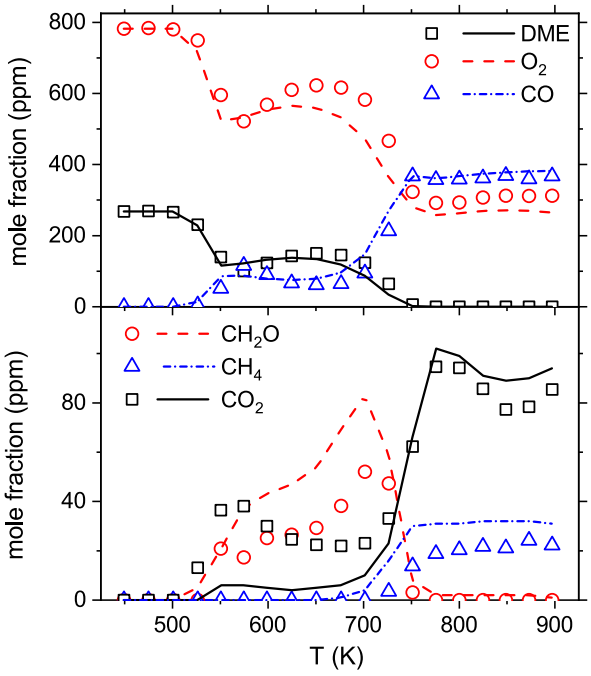

Fig. 5. Comparison of experimental and predicted concentration profiles as a function of the reactor temperature for the stoichiometric experiment with DME/O_2 (Φ=1.0). The pressure was 50 bar, and the residence time in the isothermal zone was 4.1–9.1 s. The inlet composition was 268 ppm DME, 782 ppm O_2, and N_2 by difference. The symbols mark experimental data while solid lines denote model predictions obtained with the full temperature profile.

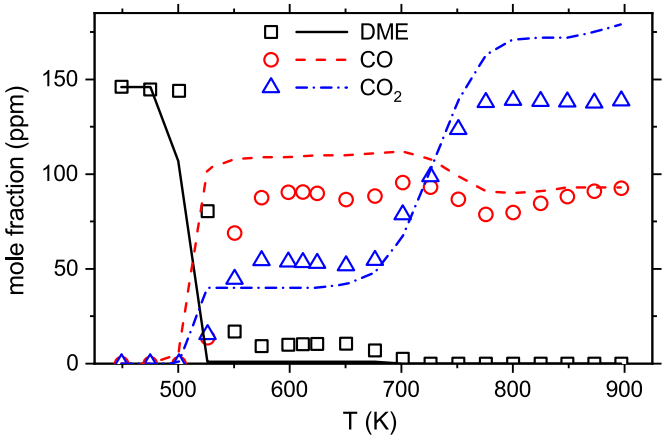

Fig. 6. Comparison of experimental and predicted concentration profiles as a function of the reactor temperature for the oxidizing experiment with DME/O_2 (Φ=0.04). The pressure was 50 bar, and the residence time in the isothermal zone was 4.1–9.1 s. The inlet composition was 146 ppm DME, 10774 ppm O_2, and N_2 by difference. The symbols mark experimental data while solid lines denote model predictions obtained with the full temperature profile.

The carbon balance for the fuel-rich experiments is closed within 11%, with the largest difference occurring at 550–575 K. According to the simulations, formic acid (HOCHO) and methyl formate (CH_3OCHO), neither of which could be measured, are formed only in trace amounts under these conditions and cannot explain the difference.

The NTC behavior of DME is more pronounced under stoichiometric conditions (Fig. 5). The onset of DME reaction is found around 525 K, where trace amounts of CO and CO_2 are detected. The NTC inflection points are observed at 575 and 650 K. Although DME is depleted above 775 K, the oxygen consumption is confined to a maximum of 60%, conceivably due to the slow oxidation of CO at these temperatures. An interesting trend in the CO_2 fraction is seen at 800–900 K, where it decreases but soon rises with elevating temperature. Methane increases monotonically with temperature and is formed in trace amounts above 725 K. Formaldehyde peaks around 700 K and disappears above 750 K.

The model predicts well the onset of reaction, the inflection points, and the mole fractions of DME, O_2, CO, and CH_4. However, the concentrations of CH_2O is overpredicted by a factor of two and CO_2 is underpredicted by almost an order of magnitude in the NTC region. The simulations indicate that under these conditions methyl formate (CH_3OCHO) and formic acid (HOCHO) are formed in significant amounts, up to 55 and 67 ppm, respectively. Adopting their mole fractions from the model, carbon is balanced within ±6%.

For the fuel-lean mixtures (Fig. 6, Φ=0.04), oxidation starts around 525 K. The NTC inflection points are positioned at 575 and 675 K. Between these points, the DME mole fraction remains almost constant but DME is depleted above 700 K. The CO mole fraction is almost independent of temperature and it stays around 90 ppm over 575–900 K.

The model predicts a slightly early onset of oxidation, but the profile shapes and concentrations of the major components are captured well. The model predicts methyl formate and formic acid to be formed in amounts of up to 15 and 106 ppm, respectively.

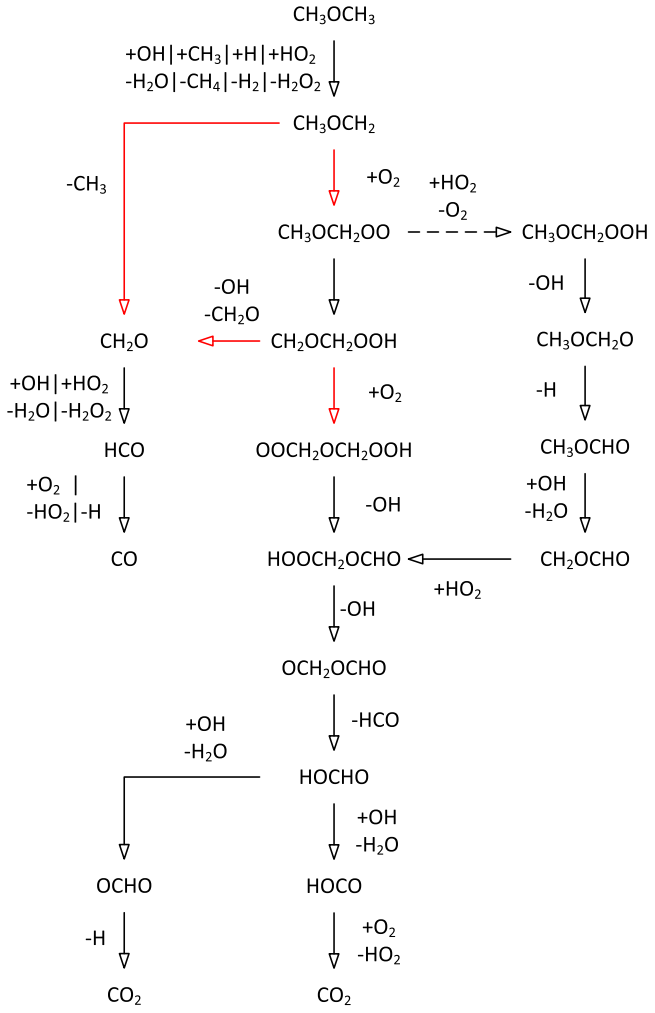

Fig. 7. The reaction pathways of DME at different stoichiometries under the flow reactor conditions at 50 bar and 550–900 K. Competing paths are marked by red lines. (For interpretation of the references to color in this figure legend, the reader is referred to the web version of this article.)

Adopting these concentrations from the model, the carbon loss in the experiments is less than 14%.

In all DME oxidization experiments, the onset temperature of DME reaction is around 525 K, independent of the fuel–air equivalence ratio. The inflection points corresponding to the NTC regime vary slightly with stoichiometry, but generally the NTC zone includes temperatures of 575–625 K. Despite differences in initial reactant concentrations and pressure, the present results are in line with the results of jet-stirred reactor [23] and flow reactor [25,35,40] experiments where DME ignition was reported around 525–550 K and the NTC zone included temperatures of 600–700 K.

Figure 7 shows the reaction pathways of DME oxidation under the flow reactor conditions. The reaction of DME with molecular oxygen (R6), and to a lesser extent the thermal decomposition of DME (R1), initiates reactions at 550–800 K. After the initiation, DME is mainly consumed by H-abstraction reactions with OH (R4), H (R2), CH_3 (R7), and HO_2 (R5) radicals. The fate of the CH_3OCH_2 radical determines to a great extent the oxidation behavior of DME. At 550 K, all CH_3OCH_2 adds to molecular oxygen to form CH_3OCH_2OO (R14a). At 650 K, around 10% of CH_3OCH_2 dissociates thermally (R13) while the contribution of this path is more than 90% at 850 K.

$$CH_3OCH_2 + O_2 = CH_3OCH_2OO \quad \text{(R14a)}$$

$$CH_3OCH_2 = CH_2O + CH_3 \quad \text{(R13)}$$

The CH_3OCH_2OO radical formed in R14a at low temperatures isomerizes to CH_2OCH_2OOH (R15a). The fate of CH_2OCH_2OOH is another critical step in the oxidation of DME; it can add to another oxygen molecule, giving $OOCH_2OCH_2OOH$ (R19), or dissociate to formaldehyde and a hydroxyl radical (R20).

$$CH_2OCH_2OOH + O_2 = OOCH_2OCH_2OOH \quad \text{(R19)}$$

$$CH_2OCH_2OOH = CH_2O + CH_2O + OH \quad \text{(R20)}$$

The second oxygen addition (R19) is favored at lower temperature whereas dissociation (R20) becomes the dominant channel at higher temperature. The low-temperature path involves the sequence $OOCH_2OCH_2OOH \rightarrow HOOCH_2OCHO \rightarrow OCH_2OCHO$, which produces two OH radicals. This chain branching sequence is responsible for the unusually high activity of DME at low temperatures. If the temperature rises from 550 K to 650 K, CH_2OCH_2OOH dissociation (R20) becomes dominant compared to the addition reaction R19. The path including R20 produces one OH radical less, so the oxidation is slowed down at 650 K. At 750 K, CH_3OCH_2 starts to dissociate (R13) instead of adding to oxygen (R14a). The path involving R13 is even less efficient in producing OH radicals.

Sensitivity coefficients for DME under the flow reactor conditions are calculated via a brute-force method in which the sensitivity coefficient (S_i) is defined as

$$S_i = \frac{(\Delta X_{DME}/X_{DME})}{(\Delta k_i/k_i)} \quad (1)$$

Figure 8 shows the results of the analysis for the stoichiometric and fuel-lean mixtures. The analysis confirms the complexity of the low temperature, high pressure oxidation chemistry of DME. Hydrogen abstraction from DME, in particular by OH (R4), HO_2 (R5), and O_2 (R6), serves to promote oxidation, while a number of peroxide-peroxide reactions, e.g., $CH_3OCH_2OO + CH_3OCH_2OO$ (R16a, R16b), $CH_3OCH_2OO + HO_2$ (R18), and $HO_2 + HO_2$, are chain terminating and slow down reaction.

As expected, the modeling predictions are sensitive to the competition between dissociation and oxygen addition for the CH_3OCH_2 and CH_2OCH_2OOH radicals,

$$CH_3OCH_2 = CH_2O + CH_3 \quad \text{(R13)}$$

$$CH_3OCH_2 + O_2 = CH_3OCH_2OO \quad \text{(R14a)}$$

$$CH_2OCH_2OOH = CH_2O + CH_2O + OH \quad \text{(R20)}$$

$$CH_2OCH_2OOH + O_2 = OOCH_2OCH_2OOH \quad \text{(R19)}$$

The addition steps, dominating at lower temperature, initiate chain branching sequences and exhibit negative sensitivity coefficients. Under oxidizing conditions, predictions are sensitive also to CH_3OCH_2OO isomerization (R15a) and decomposition of $HOOCH_2OCHO$ (R22) and $OOCH_2OCH_2OOH$ (R21) at 550 K.

$$CH_3OCH_2OO = CH_2OCH_2OOH \quad \text{(R15a)}$$

$$HOOCH_2OCHO = OCH_2OCHO + OH \quad \text{(R22)}$$

$$OOCH_2OCH_2OOH = HOOCH_2OCHO + OH \quad \text{(R21)}$$

The slightly premature onset of reaction under fuel-lean conditions (500–550 K, Fig. 6) predicted by the model is largely controlled by reactions R22, R19, R15a, and R21. Several of these reactions have

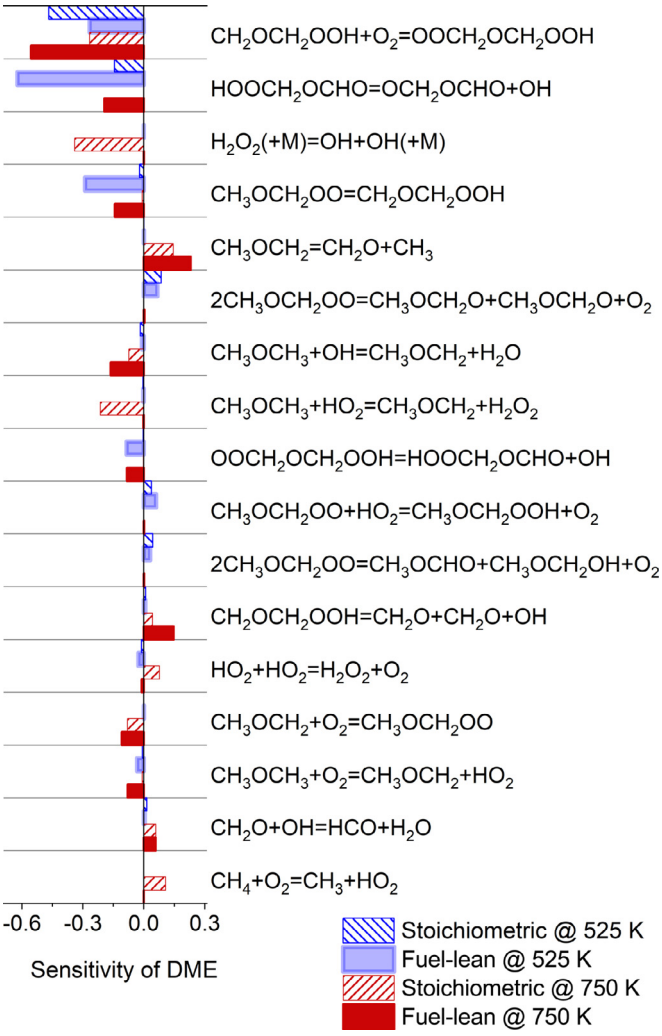

Fig. 8. Sensitivity coefficients of DME molar fraction under stoichiometric and oxidizing conditions (see captions of Figs. 5 and 6). Coefficients are calculated at time corresponding to 20% conversion of DME.

rate constants estimated with considerable uncertainty; a more accurate determination of these values could be expected to improve the model performance.

4.2. Oxidation of methane doped with DME

The effect of doping methane with small amounts of DME is investigated in the flow reactor at a pressure of 100 bar. For the neat methane, data were published previously [45] and are shown here for comparison. Figure 9 presents the results of experiments under reducing conditions (Φ=19.5–20.0). In these experiments, the inlet DME fraction fluctuated slightly ($\pm$3%), but the scatter is within the uncertainty range of the experiments. DME was added to the mixture with a DME to CH_4 ratio of 3.2%, maintaining the fuel–air equivalence ratio. Even this small amount of DME has a considerable effect, as the onset temperature of the fuel conversion shifts from $\sim$725 K for the neat methane to $\sim$575 K for the doped methane.

The DME addition affects not only the ignition temperature, but also the shapes of species profiles. For the neat DME experiment under reducing conditions, a plateau was observed in the DME profile over 575–675 K. Such a plateau now can be identified around 600–650 K for the doped experiments, not only for DME, but also for O_2, CO, and CH_4. It seems that the doped mixture inherits the two-stage ignition from DME. The first stage of ignition takes place around 575 K, a temperature higher than that of neat DME at 50 bar (525 K). The second one is around 675 K, a temperature lower than the ignition temperature of neat methane (725 K). The earlier ignition triggered by adding DME promotes the formation of CO_2 and CO at high temperatures. In contrast, C_2H_4 and C_2H_6 yields are slightly suppressed in the presence of DME.

As shown in Fig. 9, the model predicts well the onset of oxidation for the mixture as well as reproduces the NTC zone and the molar fractions of DME, O_2, CO, C_2H_4, C_2H_6, and CO_2. The only major deviations involve formaldehyde and methanol; in particular CH_2O is strongly overpredicted for the doped mixtures.

Under stoichiometric conditions (Fig. 10), two sets of experiments are conducted with DME to CH_4 ratios of 1.8% and 3.2%. For both cases, the DME conversion starts around 675 K, but there is no consumption of CH_4 and O_2 below 700–725 K. While neat methane ignites at 750 K, the addition of DME triggers methane oxidation at 25–50 K lower temperatures. The NTC behavior can be identified only in the DME profiles over 725–750 K. Apart from that, the species profiles show a monotonic trend with temperature. The major products at high temperatures are not sensibly affected by DME addition.

The model predicts well the onset of methane conversion as well as the mole fractions of O_2, CH_4, and CO, but it underestimates the ignition temperature of DME in both doped mixtures by $\sim$100 K. The prediction of the concentrations of methane and oxygen is not affected by the premature ignition of DME.

Neat DME ignites at 525 K (at 50 bar) for a wide range of stoichiometries (see Figs. 4–6), so it seems that presence of methane suppresses the ignition of DME in the mixture. This effect is not captured by the model, even though it is able to predict accurately the ignition of neat DME and neat methane under a wide range of stoichiometries. Conceivably methane activates some chain-terminating paths in DME oxidation at low temperatures that are either omitted or underpredicted by the mechanism.

For the fuel-lean mixture (Φ=0.06), the oxidation of neat methane starts around 750 K, according to Fig. 11. Doping with a DME to CH_4 ratio of 3.6% yields an onset temperature for methane oxidation at 700 K, but DME itself ignites around 625 K. The oxygen abundance promotes oxidation of CO to CO_2. The model estimates well the methane oxidation temperature as well as the fractions of CH_4, CO_2, and CO. However, DME ignition is again predicted at lower temperatures than observed, 550 K instead of 625 K.

Under stoichiometric conditions and at 725 K, ignition is only observed in the doped experiments (3.2% doping) and not in the neat methane experiments. The reaction pathway analysis reveals that the DME conversion here is initiated by the reaction between DME and molecular oxygen, similar to neat DME (Fig. 7). The produced CH_3OCH_2 radical then follows the consumption path of neat DME, yielding OH radicals, especially from the dissociation of CH_2OCH_2OOH at this temperature. At an early stage of ignition, around two-thirds of the produced OH radicals are consumed by reaction with methane,

$$CH_4 + OH = CH_3 + H_2O \qquad (R26)$$

which starts the major path of methane oxidation. After ignition, methane follows the consumption path of neat methane as described in [45].

At 550 K, DME should not be oxidized according to the measurements (Figs. 10 and 11), but the model predicts a considerable consumption of DME. The overall fuel to oxygen ratio corresponds to a stoichiometric mixture, but DME reacts in an excess oxygen environment since methane apparently does not participate in the oxidation at such a low temperature. A sensitivity analysis for prediction of DME at 550 K for both stoichiometric and oxidizing

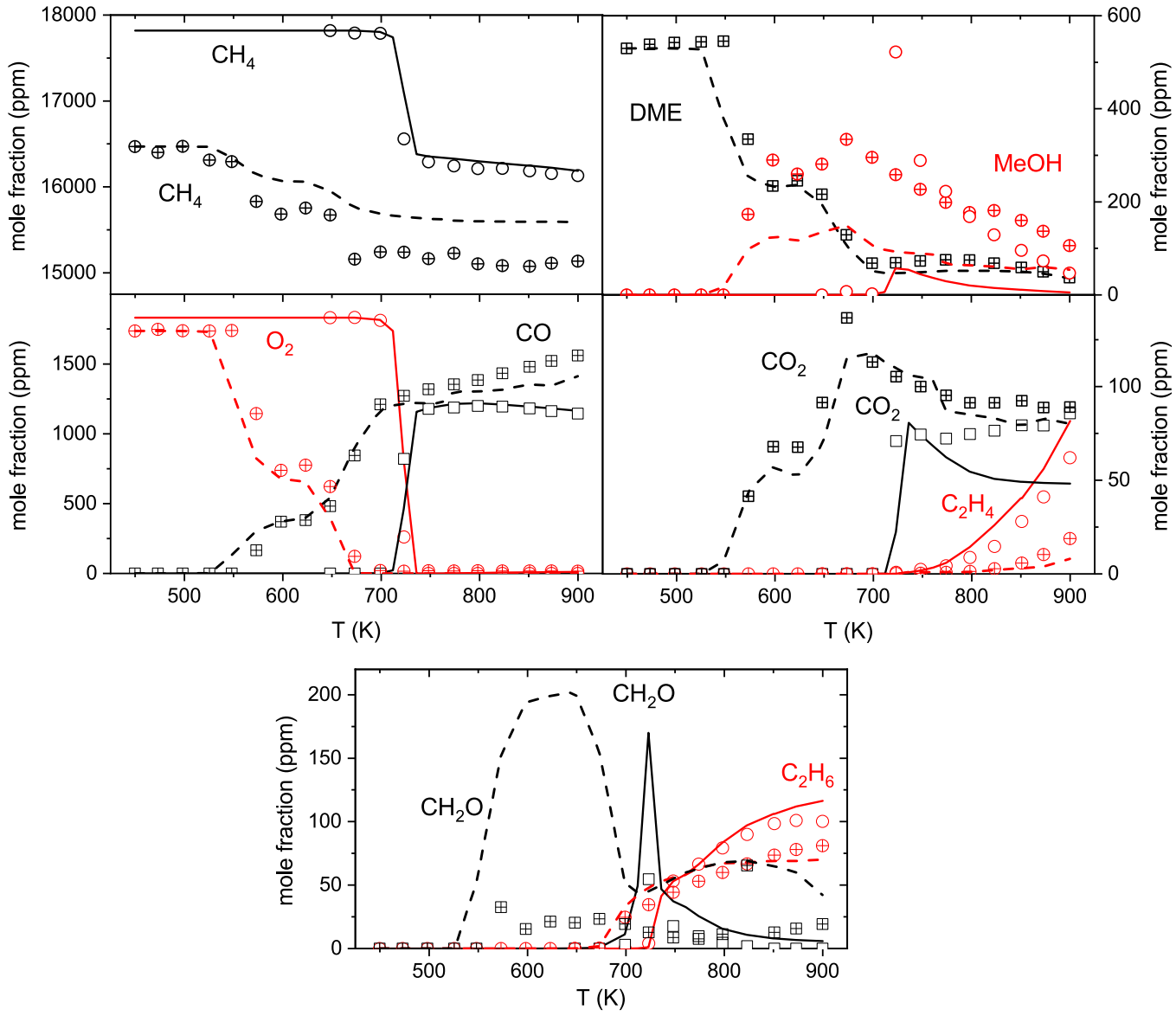

Fig. 9. Comparison of experimental and predicted concentration profiles as a function of the reactor temperature for DME addition to methane under reducing conditions (Φ=19.5–20.0) and at 100 bar. Open symbols/solid lines: the neat CH_4 experiment [45] with 17,820 ppm CH_4 and 1832 ppm O_2; crossed symbols/dashed lines: the doped experiment with 16,470 ppm CH_4, 530 ppm DME and 1736 ppm O_2; all diluted in N_2. For neat as well as for the doped methane experiments, the isothermal residence time is given by $\tau[s] = 9550/T[K]$.

mixtures of the doped methane (3.2% and 3.6% doping) is shown in Fig. 12. The onset of reaction for DME is particularly sensitive to the competition for OH radicals between DME and CH_4,

$$CH_3OCH_3 + OH = CH_3OCH_2 + H_2O \quad (R4)$$

$$CH_4 + OH = CH_3 + H_2O \quad (R26)$$

The rate constants for both of these reactions are known with little uncertainty and they are unlikely to be the source of discrepancy in the modeling. Other reactions showing up in the sensitivity analysis, including

$$HOOCH_2OCHO = OCH_2OCHO + OH \quad (R22)$$

$$CH_3OCH_3 + O_2 = CH_3OCH_2 + HO_2 \quad (R6)$$

may be more uncertain but exhibit smaller sensitivity coefficients.

4.3. Comparison with literature data

The mechanism prediction was compared against literature data from flame speed measurements and data from flow reactors; results generally obtained at pressures lower than those found in engines. The details of comparison can be found in the Supplementary material. The model reproduces accurately flame speeds for DME at pressures up to 10 atm. Flow-reactor data from literature on DME oxidation are also captured reasonably by the model at pressures up to 18 atm. As high-pressure application is the focus of this study, we discuss high-pressure ignition delays in more detail in this section.

4.3.1. Ignition delays

The model can be evaluated at higher temperatures by comparing its prediction with available ignition delays measured in shock tubes. The ignition delay times of stoichiometric DME/air and DME/O_2/Ar at pressures of 1–40 bar are shown in Fig. 13. As

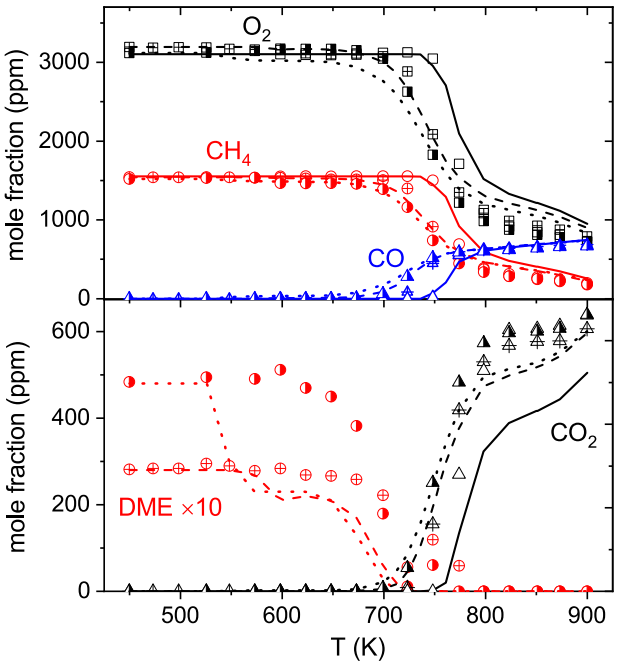

Fig. 10. Comparison of experimental and predicted concentration profiles as a function of the reactor temperature for DME addition to methane under stoichiometric conditions (Φ=0.99–1.02) and at 100 bar. Open symbols/solid lines: the neat CH_4 experiment [45] with 1550 ppm CH_4 and 3100 ppm O_2; crossed symbols/dashed lines: the doped experiment (1.8%) with 1540 ppm CH_4, 28 ppm DME and 3195 ppm O_2; half-open symbols/dotted lines: the doped experiment (3.2%) with 1520 ppm CH_4, 48 ppm DME and 3320 ppm O_2; all diluted in N_2. For neat as well as for the doped methane experiments, the isothermal residence time is given by $\tau[s] = 9550/T[K]$.

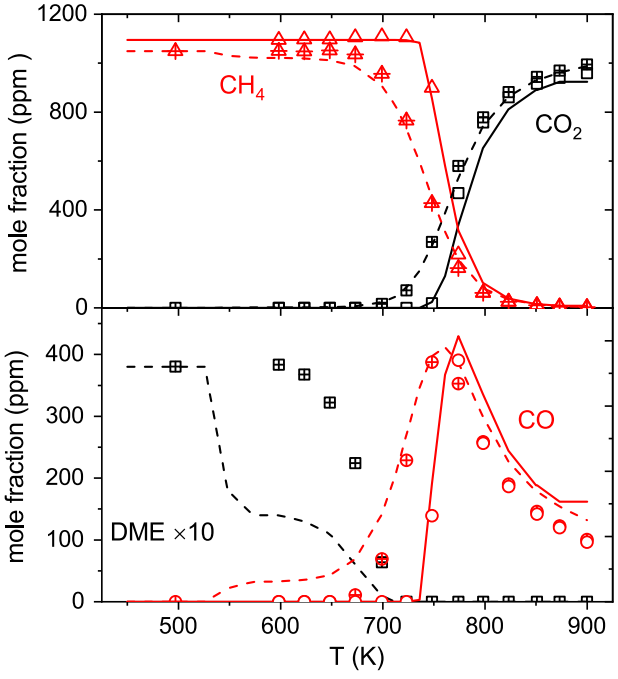

Fig. 11. Comparison of experimental and predicted concentration profiles as a function of the reactor temperature for DME addition to methane under oxidizing conditions (Φ=0.06) and at 100 bar. Open symbols/solid lines: the neat CH_4 experiment [45] with 1100 ppm CH_4 and 39,600 ppm O_2; crossed symbols/dashed lines: the doped experiment with 1050 ppm CH_4, 38 ppm DME and 36,850 ppm O_2; all diluted in N_2. For neat as well as for the doped methane experiments, the isothermal residence time is given by $\tau[s] = 9550/T[K]$.

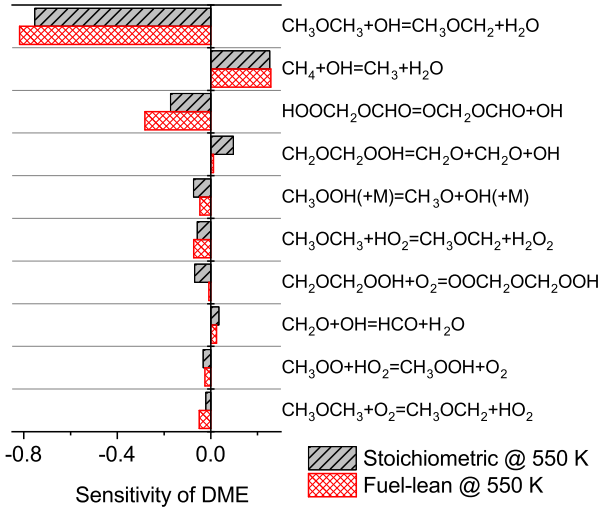

Fig. 12. Sensitivity of DME molar fraction under stoichiometric (DME/CH_4=3.2 %) and oxidizing (DME /CH_4=3.6 %) conditions (100 bar, 550 K) in the flow reactor. Coefficients are calculated at time corresponding to 20% conversion of DME.

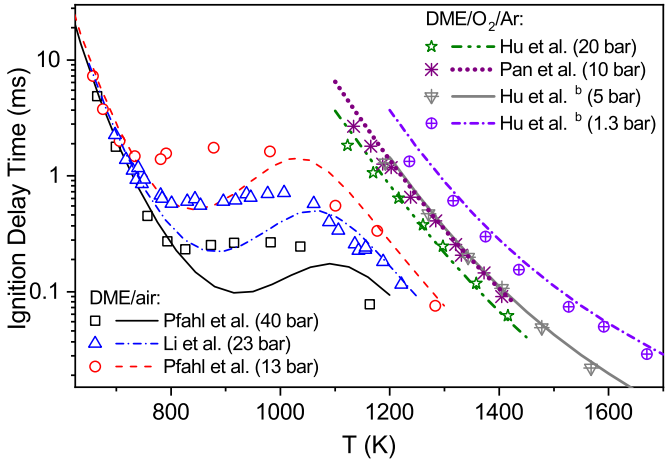

Fig. 13. Ignition delay times of stoichiometric DME/air (data from Pfahl et al. [22] and Li et al. [27]) and DME/O_2/Ar (data from Hu et al. [10], Pan et al. [73], Hu et al.[b] [74]). Lines denote the prediction of the present model assuming a constant-volume adiabatic system.

expected, DME/air ignites considerably faster than the more dilute mixtures of DME/O_2/Ar. The ignition delays of DME/air are characterized by two inflection points, representing NTC behavior. The first inflection point increases from 790 K to 830 K when pressure is increased from 13 bar to 40 bar. The sensitivity of ignition delay to pressure is higher in the NTC region, where increasing pressure reduces the ignition delay considerably. The model reproduces well the ignition delays below the first inflection point ($T < 800$ K) and above the second one ($T > \sim 1000$ K), but it strongly underestimates ignition delays between inflection points.

The ignition delay times of mixtures diluted in argon are measured at temperatures above 1100 K, so NTC behavior is not expected. Here, pressure has an accelerating effect on ignition and the model agrees well with the measurements in Fig. 13.

The model is further evaluated against ignition delays under fuel-rich and fuel-lean conditions for the diluted mixtures of DME/O_2 in argon or nitrogen (Fig. 14). The ignition delays are longer for the fuel-lean mixtures. As for stoichiometric conditions, the model predicts well the ignition delays outside NTC zone, while the IDT in the NTC region is strongly underpredicted. A number of literature models, e.g., [13,24,28,33], offer more

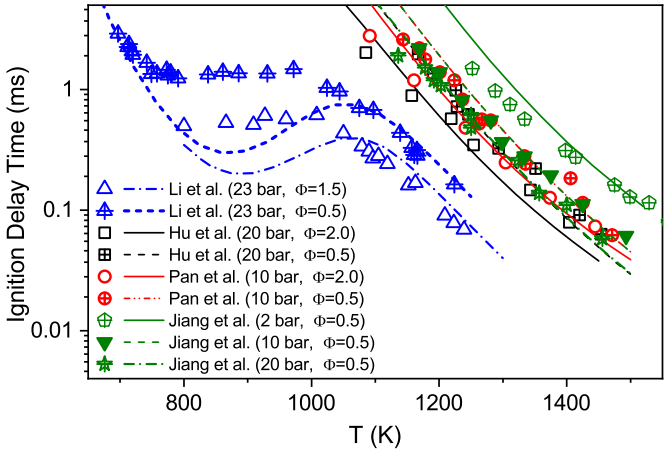

Fig. 14. Ignition delay times of fuel-lean (Hu et al. [10]: 0.68% DME in O_2/Ar, Li et al. [27]: 3.38% DME in O_2/N_2, Pan et al. [73]: 0.68% DME in O_2/Ar) and fuel-rich (Hu et al. [10]: 2.46% DME in O_2/Ar, Li et al. [27]: 9.51% DME in O_2/N_2, Pan et al. [73]: 2.46% DME in O_2/Ar) mixtures at different pressures. Lines denote the prediction of the present model assuming a constant-volume adiabatic system.

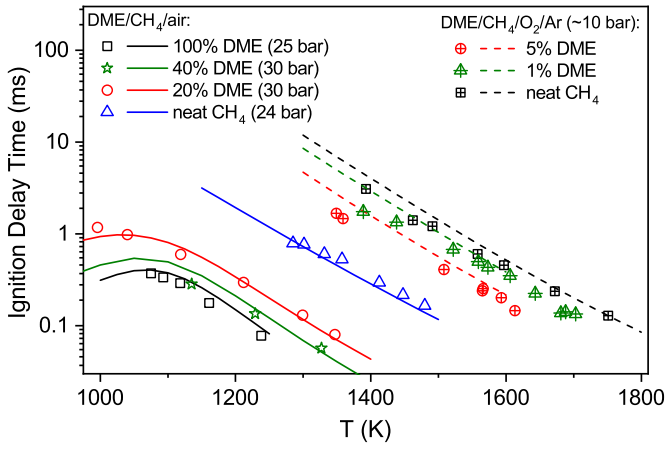

Fig. 15. Effect of replacing methane by DME on the ignition delay times of stoichiometric mixtures. Symbols present the measurements in shock tubes for mixtures in air by Burke et al. [28] and for mixtures in argon (94% AR) by Tang et al. [9]. Lines denote the prediction of the present model assuming constant-volume adiabatic system.

accurate predictions of the ignition delays in the NTC zone, but the improved agreement comes at the cost of using less accurate rate constants for reactions in the CH_3OCH_2OO system. Further work is desirable to reconcile this issue.

Previously we observed that the model was able to predict accurately the onset temperature of the major reaction in the mixtures of methane and DME in the flow reactor although it predicted premature ignition of DME in the mixtures. To further evaluate the interaction of methane and DME in the model, the ignition delays of mixtures of methane and DME are calculated and compared to reported data in Fig. 15. Here, the DME to methane ratio is varied from 0% to 100%, and as can be seen the model follows very well the experimental results for mixtures in air. For the mixtures in argon, the model estimates slightly longer ignition delays compared to the measurements.

Sensitivity of ignition delays of DME/air to reaction rate constants are calculated using the brute-force method and is shown in Fig. 16. The dissociation of CH_3OCH_2 (R13) is the most important reaction for ignition delays at 900/1100 K. Increasing the rate of this reaction prolongs the ignition delays considerably. Isomerization of CH_3OCH_2OO (R15a) accelerates ignition at 700–1100 K.

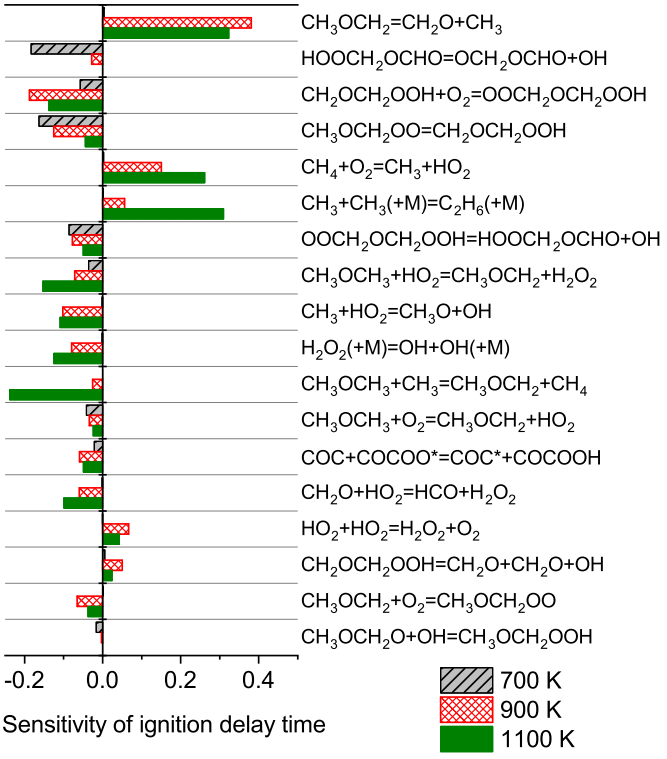

Fig. 16. Sensitivity of ignition delay time of DME/air (stoichiometric mixture) to reaction rate constants. The coefficients were calculated at a pressure of 40 bar and at different temperatures. COC+COCOO*=COC*+COCOOH represents $CH_3OCH_3 + CH_3OCH_2OO = CH_3OCH_2 + CH_3OCH_2OOH$.

The chain-terminating reactions of R28rev and R29 inhibit ignition considerably at 900/1100 K.

$$CH_3 + HO_2 = CH_4 + O_2 \quad \text{(R28rev)}$$

$$CH_3 + CH_3(+M) = C_2H_6(+M) \quad \text{(R29)}$$

At 700 K, dissociation of $HOOCH_2OCHO$ (R22) is the most critical step for the ignition delay prediction.

$$HOOCH_2OCHO = OCH_2OCHO + OH \quad \text{(R22)}$$

As discussed earlier, the rate of this reaction has been estimated with a large uncertainty.

5. Conclusion

The pyrolysis and oxidation of DME and its effect as an additive on methane oxidation have been investigated in a flow reactor at high pressures and intermediate temperatures. The presented species profiles from DME and DME/CH_4 conversion extend the experimental benchmark for oxidation at high pressures and intermediate temperatures. At 50 bar, pyrolysis of DME started around 825 K, while onset of oxidation was detected at 525 K, independent of fuel–air equivalence ratio. Adding a small amount of DME to methane at 100 bar effectively accelerated its ignition, most pronounced under reducing conditions. A model was developed for DME/CH_4 oxidation and evaluated over a wide range of pressure, temperature, and stoichiometry. Modeling predictions compared well with the data for neat DME oxidation from the flow reactor. Also ignition delays and flame speeds of DME were predicted well under most of the investigated conditions, but calculations of ignition delays between the NTC inflection points were less accurate. For CH_4/DME mixtures, the model captured well the onset of reaction for CH_4, but predicted premature depletion of DME.

Further work is desirable to reconcile experimental and theoretical work on reactions on the CH_3OCH_2OO PES with ignition delay measurements in the NTC region for DME. Moreover, work is required to improve understanding of the interactions between DME and CH_4, in particular the inhibiting effect of methane on DME oxidation.

Acknowledgment

Funding from the European Graduate School as well as MAN Energy Solutions is gratefully acknowledged. This project has received funding from the European Union's Horizon 2020 research and innovation program under grant agreement no. 634135 HERCULES-2.

Supplementary material

Supplementary material associated with this article can be found, in the online version, at doi:10.1016/j.combustflame.2019.03.028.

References

[1] D. Cipolat, Analysis of energy release and NO_x emissions of a CI engine fuelled on diesel and DME, Appl. Therm. Eng. 27 (11–12) (2007) 2095–2103.
[2] C. Arcoumanis, C. Bae, R. Crookes, E. Kinoshita, The potential of di-methyl ether (DME) as an alternative fuel for compression-ignition engines: a review, Fuel 87 (7) (2008) 1014–1030.
[3] G. Thomas, B. Feng, A. Veeraragavan, M.J. Cleary, N. Drinnan, Emissions from DME combustion in diesel engines and their implications on meeting future emission norms: a review, Fuel Process. Technol. 119 (2014) 286–304.
[4] S. Sidhu, J. Graham, R. Striebich, Semi-volatile and particulate emissions from the combustion of alternative diesel fuels, Chemosphere 42 (5–7) (2001) 681–690.
[5] L. Xinling, H. Zhen, Emission reduction potential of using gas-to-liquid and dimethyl ether fuels on a turbocharged diesel engine, Sci. Total Environ. 407 (7) (2009) 2234–2244.
[6] M.C. Lee, S.B. Seo, J.H. Chung, Y.J. Joo, D.H. Ahn, Industrial gas turbine combustion performance test of DME to use as an alternative fuel for power generation, Fuel 88 (4) (2009) 657–662.
[7] T. Amano, F.L. Dryer, Effect of dimethyl ether, NO_x, and ethane on CH_4 oxidation: high pressure, intermediate-temperature experiments and modeling, Symp. (Int.) Combust. 27 (1) (1998) 397–404.
[8] Z. Chen, X. Qin, Y. Ju, Z. Zhao, M. Chaos, F.L. Dryer, High temperature ignition and combustion enhancement by dimethyl ether addition to methane–air mixtures, Proc. Combust. Inst. 31 (1) (2007) 1215–1222.
[9] C. Tang, L. Wei, J. Zhang, X. Man, Z. Huang, Shock tube measurements and kinetic investigation on the ignition delay times of methane/dimethyl ether mixtures, Energy Fuels 26 (11) (2012) 6720–6728.
[10] E. Hu, Z. Zhang, L. Pan, J. Zhang, Z. Huang, Experimental and modeling study on ignition delay times of dimethyl ether/propane/oxygen/argon mixtures at 20 bar, Energy Fuels 27 (7) (2013) 4007–4013.
[11] F. Sen, B. Shu, T. Kasper, J. Herzler, O. Welz, M. Fikri, B. Atakan, C. Schulz, Shock-tube and plug-flow reactor study of the oxidation of fuel-rich CH_4/O_2 mixtures enhanced with additives, Combust. Flame 169 (2016) 307–320.
[12] W.B. Lowry, Z. Serinyel, M.C. Krejci, H.J. Curran, G. Bourque, E.L. Petersen, Effect of methane-dimethyl ether fuel blends on flame stability, laminar flame speed, and Markstein length, Proc. Combust. Inst. 33 (1) (2011) 929–937.
[13] C.B. Reuter, R. Zhang, O.R. Yehia, Y. Rezgui, Y. Ju, Counterflow flame experiments and chemical kinetic modeling of dimethyl ether/methane mixtures, Combust. Flame 196 (2018) 1–10.
[14] S.S. Yoon, D.H. Anh, S.H. Chung, Synergistic effect of mixing dimethyl ether with methane, ethane, propane, and ethylene fuels on polycyclic aromatic hydrocarbon and soot formation, Combust. Flame 154 (3) (2008) 368–377.
[15] D. Lee, J.S. Lee, H.Y. Kim, C.K. Chun, S.C. James, S.S. Yoon, Experimental study on the combustion and NO_x emission characteristics of DME/LPG blended fuel using counterflow burner, Combust. Sci. Technol. 184 (1) (2012) 97–113.
[16] D. Cipolat, N. Bhana, Fuelling of a compression ignition engine on ethanol with DME as ignition promoter: effect of injector configuration, Fuel Process. Technol. 90 (9) (2009) 1107–1113.
[17] C. Liang, C. Ji, B. Gao, X. Liu, Y. Zhu, Investigation on the performance of a spark-ignited ethanol engine with DME enrichment, Energy Convers. Manag. 58 (0) (2012) 19–25.
[18] C.J. Green, N.A. Cockshutt, L. King, Dimethyl ether as a methanol ignition improver: substitution requirements and exhaust emissions impact, SAE International (1990). SAE Technical Paper 902155
[19] M.E. Karpuk, J.D. Wright, J.L. Dippo, D.E. Jantzen, Dimethyl ether as an ignition enhancer for methanol-fueled diesel engines, SAE International (1991). SAE Technical Paper 912420
[20] M.E. Karpuk, S.W. Cowley, On board dimethyl ether generation to assist methanol engine cold starting, SAE Technical Paper 881678, SAE International (1998).
[21] J. Zhang, E. Hu, L. Pan, Z. Zhang, Z. Huang, Shock-tube measurements of ignition delay times for the ethane/dimethyl ether blends, Energy Fuels 27 (10) (2013) 6247–6254.
[22] U. Pfahl, K. Fieweger, G. Adomeit, Self-ignition of diesel-relevant hydrocarbon-air mixtures under engine conditions, Symp. (Int.) Combust. 26 (1) (1996) 781–789.
[23] P. Dagaut, C. Daly, J.M. Simmie, M. Cathonnet, The oxidation and ignition of dimethylether from low to high temperature (500–1600 K): experiments and kinetic modeling, Symp. (Int.) Combust. 27 (1) (1998) 361–369.
[24] Z. Zhao, M. Chaos, A. Kazakov, F.L. Dryer, Thermal decomposition reaction and a comprehensive kinetic model of dimethyl ether, Int. J. Chem. Kinet. 40 (1) (2008) 1–18.
[25] H.J. Curran, S.L. Fischer, F.L. Dryer, The reaction kinetics of dimethyl ether. II: low-temperature oxidation in flow reactors, Int. J. Chem. Kinet. 32 (12) (2000) 741–759.
[26] S.H. Won, B. Windom, B. Jiang, Y. Ju, The role of low temperature fuel chemistry on turbulent flame propagation, Combust. Flame 161 (2) (2014) 475–483.
[27] Z. Li, W. Wang, Z. Huang, M.A. Oehlschlaeger, Dimethyl ether autoignition at engine-relevant conditions, Energy Fuels 27 (5) (2013) 2811–2817.
[28] U. Burke, K.P. Somers, P. O'Toole, C.M. Zinner, N. Marquet, G. Bourque, E.L. Petersen, W.K. Metcalfe, Z. Serinyel, H.J. Curran, An ignition delay and kinetic modeling study of methane, dimethyl ether, and their mixtures at high pressures, Combust. Flame 162 (2) (2015) 315–330.
[29] D. Liu, J. Santner, C. Togbé, D. Felsmann, J. Koppmann, A. Lackner, X. Yang, X. Shen, Y. Ju, K. Kohse-Höinghaus, Flame structure and kinetic studies of carbon dioxide-diluted dimethyl ether flames at reduced and elevated pressures, Combust. Flame 160 (12) (2013) 2654–2668.
[30] X. Qin, Y.G. Ju, Measurements of burning velocities of dimethyl ether and air premixed flames at elevated pressures, Proc. Combust. Inst. 30 (1) (2005) 233–240.
[31] J. de Vries, W.B. Lowry, Z. Serinyel, H.J. Curran, E.L. Petersen, Laminar flame speed measurements of dimethyl ether in air at pressures up to 10 atm, Fuel 90 (1) (2011) 331–338.
[32] P. Dagaut, J.-C. Boettner, M. Cathonnet, Chemical kinetic study of dimethylether oxidation in a jet stirred reactor from 1 to 10 atm: experiments and kinetic modeling, Symp. (Int.) Combust. 26 (1) (1996) 627–632.
[33] A. Rodriguez, O. Frottier, O. Herbinet, R. Fournet, R. Bounaceur, C. Fittschen, F. Battin-Leclerc, Experimental and modeling investigation of the low-temperature oxidation of dimethyl ether, J. Phys. Chem. A 119 (28) (2015) 7905–7923.
[34] K. Moshammer, A.W. Jasper, D.M. Popolan-Vaida, A. Lucassen, P. Diévart, H. Selim, A.J. Eskola, C.A. Taatjes, S.R. Leone, S.M. Sarathy, Y. Ju, P. Dagaut, K. Kohse-Höinghaus, N. Hansen, Detection and identification of the keto-hydroperoxide ($HOOCH_2OCHO$) and other intermediates during low-temperature oxidation of dimethyl ether, J. Phys. Chem. A 119 (28) (2015) 7361–7374.
[35] F. Herrmann, P. Oßwald, K. Kohse-Höinghaus, Mass spectrometric investigation of the low-temperature dimethyl ether oxidation in an atmospheric pressure laminar flow reactor, Proc. Combust. Inst. 34 (1) (2013) 771–778.
[36] F. Herrmann, B. Jochim, P. Oßwald, L. Cai, H. Pitsch, K. Kohse-Höinghaus, Experimental and numerical low-temperature oxidation study of ethanol and dimethyl ether, Combust. Flame 161 (2) (2014) 384–397.
[37] N. Kurimoto, B. Brumfield, X. Yang, T. Wada, P. Diévart, G. Wysocki, Y. Ju, Quantitative measurements of HO_2/H_2O_2 and intermediate species in low and intermediate temperature oxidation of dimethyl ether, Proc. Combust. Inst. 35 (1) (2015) 457–464.
[38] S.L. Fischer, F.L. Dryer, H.J. Curran, The reaction kinetics of dimethyl ether: I. High-temperature pyrolysis and oxidation in flow reactors, Int. J. Chem. Kinet. 32 (12) (2000) 713–740.
[39] G. Mittal, M. Chaos, C.-J. Sung, F.L. Dryer, Dimethyl ether autoignition in a rapid compression machine: experiments and chemical kinetic modeling, Fuel Process. Technol. 89 (12) (2008) 1244–1254.
[40] L. Marrodán, Á.J. Arnal, Á. Millera, R. Bilbao, M.U. Alzueta, The inhibiting effect of NO addition on dimethyl ether high-pressure oxidation, Combust. Flame 197 (2018) 1–10.
[41] E.E. Dames, A.S. Rosen, B.W. Weber, C.W. Gao, C.-J. Sung, W.H. Green, A detailed combined experimental and theoretical study on dimethyl ether/propane blended oxidation, Combust. Flame 168 (2016) 310–330.
[42] M.U. Alzueta, J. Muro, R. Bilbao, P. Glarborg, Oxidation of dimethyl ether and its interaction with nitrogen oxides, Isr. J. Chem. 39 (1) (1999) 73–86.
[43] H.J. Curran, W.J. Pitz, C.K. Westbrook, P. Dagaut, J.C. Boettner, M. Cathonnet, A wide range modeling study of dimethyl ether oxidation, Int. J. Chem. Kinet. 30 (3) (1998) 229–241.
[44] H. Hashemi, J.M. Christensen, S. Gersen, P. Glarborg, Hydrogen oxidation at high pressure and intermediate temperatures: experiments and kinetic modeling, Proc. Combust. Inst. 35 (1) (2015) 553–560.
[45] H. Hashemi, J.M. Christensen, S. Gersen, H. Levinsky, S.J. Klippenstein, P. Glarborg, High-pressure oxidation of methane, Combust. Flame 172 (2016) 349–364.
[46] H. Hashemi, J.G. Jacobsen, C.T. Rasmussen, J.M. Christensen, P. Glarborg, S. Gersen, M. van Essen, H.B. Levinsky, S.J. Klippenstein, High-pressure oxidation of ethane, Combust. Flame 182 (2017) 150–166.

[47] V. Aranda, J.M. Christensen, M.U. Alzueta, P. Glarborg, S. Gersen, Y. Gao, P. Marshall, Experimental and kinetic modeling study of methanol ignition and oxidation at high pressure, Int. J. Chem. Kinet. 45 (5) (2013) 283–294.
[48] J. Lopez, C. Rasmussen, H. Hashemi, M. Alzueta, Y. Gao, P. Marshall, C. Goldsmith, P. Glarborg, Experimental and kinetic modeling study of C_2H_2 oxidation at high pressure, Int. J. Chem. Kinet. 48 (11) (2016) 724–738.
[49] H. Hashemi, J.M. Christensen, P. Glarborg, High-pressure pyrolysis and oxidation of ethanol, Fuel 218 (2018) 247–257.
[50] A.S. Tomlin, E. Agbro, V. Nevrly, J. Dlabka, M. Vasinek, Evaluation of combustion mechanisms using global uncertainty and sensitivity analyses: a case study for low-temperature dimethyl ether oxidation, Int. J. Chem. Kinet. 46 (2014) 662–682.
[51] A.J. Eskola, S.A. Carr, R.J. Shannon, B. Wang, M.A. Blitz, M.J. Pilling, P.W. Seakins, S.H. Robertson, Analysis of the kinetics and yields of OH radical production from the $CH_3OCH_2 + O_2$ reaction in the temperature range 195–650 K: an experimental and computational study, J. Phys. Chem. A 118 (34) (2014) 6773–6788.
[52] R.J. Shannon, A.S. Tomlin, S.H. Robertson, M.A. Blitz, M.J. Pilling, P.W. Seakins, Global uncertainty propagation and sensitivity analysis in the $CH_3OCH_2 + O_2$ system: combining experiment and theory to constrain key rate coefficients in DME combustion, J. Phys. Chem. A 119 (2015) 7430–7438.
[53] C.L. Rasmussen, J. Hansen, P. Marshall, P. Glarborg, Experimental measurements and kinetic modeling of $CO/H_2/O_2/NO$, conversion at high pressure, Int. J. Chem. Kinet. 40 (8) (2008) 454–480.
[54] Ansys 19.0 Chemkin, (2018).
[55] P. Marshall, P. Glarborg, Ab initio and kinetic modeling studies of formic acid oxidation, Proc. Combust. Inst. 35 (1) (2015) 153–160.
[56] A.B. Elke Goos, B. Ruscic, Extended third millenium ideal gas thermochemical database with updates from active thermochemical tables (2016) http://garfield.chem.elte.hu/Burcat/burcat.html.
[57] C.F. Goldsmith, W.H. Green, S.J. Klippenstein, Role of $O_2 + QOOH$ in low-temperature ignition of propane: 1. Temperature and pressure dependent rate coefficients, J. Phys. Chem. A 116 (13) (2012) 3325–3346.
[58] C.W. Gao, J.W. Allen, W.H. Green, R.H. West, RMG database (reaction mechanism generator: automatic construction of chemical kinetic mechanisms), Comput. Phys. Commun. 203 (2016) 212–225. See also RMG database (http://rmg.mit.edu)
[59] R. Sivaramakrishnan, J.V. Michael, A.F. Wagner, R. Dawes, A.W. Jasper, L.B. Harding, Y. Georgievskii, S.J. Klippenstein, Roaming radicals in the thermal decomposition of dimethyl ether: experiment and theory, Combust. Flame 158 (4) (2011) 618–632.
[60] R.S. Tranter, P.T. Lynch, X. Yang, Dissociation of dimethyl ether at high temperatures, Proc. Combust. Inst. 34 (1) (2013) 591–598.
[61] S.A. Carr, T.J. Still, M.A. Blitz, A.J. Eskola, M.J. Pilling, P.W. Seakins, R.J. Shannon, B. Wang, S.H. Robertson, Experimental and theoretical study of the kinetics and mechanism of the reaction of OH radicals with dimethyl ether, J. Phys. Chem. A 117 (44) (2013) 11142–11154.
[62] R.S. Tranter, P.T. Lynch, C.J. Annesley, Shock tube investigation of $CH_3 + CH_3OCH_3$, J. Phys. Chem. A 116 (27) (2012) 7287–7292.
[63] H. Hashemi, J.M. Christensen, L.B. Harding, S.J. Klippenstein, P. Glarborg, High–pressure oxidation of propane, Proc. Combust. Inst. 37 (1) (2019) 461–468.
[64] J. Mendes, C.-W. Zhou, H.J. Curran, Rate constant calculations of H-atom abstraction reactions from ethers by HO_2 radicals, J. Phys. Chem. A 118 (8) (2014) 1300–1308.
[65] H.-H. Carstensen, A.M. Dean, O. Deutschmann, Rate constants for the H abstraction from alkanes (R–H) by $R'O_2$ radicals: a systematic study on the impact of R and R′, Proc. Combust. Inst. 31 (1) (2007) 149–157.
[66] L.F. Loucks, K.J. Laidler, Mercury-photosensitized decomposition of dimethyl ether: part II. The thermal decomposition of the methoxymethyl radical, Can. J. Chem. 45 (1967) 2767–2773.
[67] J. Sehested, K. Sehested, J. Platz, H. Egsgaard, O.J. Nielsen, Oxidation of dimethyl ether: absolute rate constants for the self reaction of CH_3OCH_2 radicals, the reaction of CH_3OCH_2 radicals with O_2, and the thermal decomposition of CH_3OCH_2 radicals, Int. J. Chem. Kinet. 29 (1997) 627–636.
[68] J. Gao, Y. Guan, J. Lou, H. Ma, J. Song, Kinetic modeling for unimolecular β-scission of the methoxymethyl radical from quantum chemical and RRKM analyses, Combust. Flame 197 (2018) 243–253.
[69] A. Andersen, E.A. Carter, Hybrid density functional theory predictions of low-temperature dimethyl ether combustion pathways: II. Chain-branching energetics and possible role of the Criegee intermediate, J. Phys. Chem. 107 (2003) 9463–9478.
[70] A. Andersen, E.A. Carter, First-principles-derived kinetics of the reactions involved in low-temperature dimethyl ether oxidation, Mol. Phys. 106 (2008) 367–396.
[71] S. Dooley, M.P. Burke, M. Chaos, Y. Stein, F.L. Dryer, V.P. Zhukov, O. Finch, J.M. Simmie, H.J. Curran, Methyl formate oxidation: speciation data, laminar burning velocities, ignition delay times, and a validated chemical kinetic model, Int. J. Chem. Kinet. 42 (9) (2010) 527–549.
[72] Y. Guan, Y. Li, L. Zhao, Y. Song, H. Ma, J. Song, Hydrogen transfer between dimethyl ether and the methoxy radical: understanding and kinetic modeling with anharmonic torsions, Comput. Theor. Chem. 1089 (2016) 43–53.
[73] L. Pan, E. Hu, J. Zhang, Z. Zhang, Z. Huang, Experimental and kinetic study on ignition delay times of $DME/H_2/O_2/Ar$ mixtures, Combust. Flame 161 (3) (2014) 735–747.
[74] E. Hu, X. Jiang, Z. Huang, J. Zhang, Z. Zhang, X. Man, Experimental and kinetic studies on ignition delay times of Dimethyl Ether/n-Butane/O_2/Ar mixtures, Energy Fuels 27 (1) (2013) 530–536.